

¹ **Sub-grid scale turbulent micro-mixing with infinitely fast chemistry in the context of fire
2 modelling**

³ Georgios Maragkos*, Bart Merci*

⁴ Department of Structural Engineering and Building Materials, Ghent University, Technologiepark-
⁵ Zwijnaarde 60, 9052 Zwijnaarde, Belgium.

⁶* Corresponding author. Emails: Georgios.Maragkos@UGent.be, Bart.Merci@UGent.be

⁷ **Highlights:**

- ⁸ • Six different micro-mixing models with infinitely fast chemistry are tested
⁹ • The model using an effective diffusion time scale was highly grid-sensitive
¹⁰ • The differences between the models were more pronounced on coarser grid sizes

¹¹ **Abstract:**

¹² Combustion modelling with the Eddy Dissipation Model (EDM) requires closure of the mixing
¹³ time between fuel and oxidizer occurring on a sgs level. Six different models for estimating the
¹⁴ micro-mixing times, in the context of fire modelling, are investigated: 1) equal to a constant fraction
¹⁵ of the integral time scale (i.e., default EDM approach); 2) allow for this fraction to vary in space
¹⁶ and time as a function of the standard deviation of the mixture fraction; 3) use of the geometric
¹⁷ mean of the integral time scale and the Kolmogorov time scale; 4) use of the geometric mean of the
¹⁸ sub-grid velocity stretching time and the Kolmogorov time scale; 5) calculation of the mixing time
¹⁹ scale based on the local variation of the scalar dissipation rate and the mixture fraction variance;
²⁰ 6) use of the minimum of the mixing times for diffusion, sub-grid scale advection and buoyant
²¹ acceleration. Overall, the performance of all models on fine grids is comparable. However, models
²² 2 and 6 perform better for all the grid sizes and test cases considered. Model 1 predicts the highest
²³ temperatures, the performance of models 3 and 4 is similar while the predictions with model 5 are
²⁴ highly grid-dependent.

²⁵ **Keywords:** micro-mixing; combustion; EDM; LES; fire

²⁶ **1. Introduction**

²⁷ Fires represent a significant hazard in today's society, with potential impact on human lives and
²⁸ properties, given the abundance of combustible materials found on and in buildings and in nature.
²⁹ Progress in fire safety science is, nowadays, strongly assisted by the use of Computational Fluid
³⁰ Dynamics (CFD). CFD has also become a valuable tool in the hands of fire safety engineers. As such,
³¹ there is need for numerical models that can accurately simulate a plethora of fire-related scenarios
³² (e.g., involving smoke transport, flame spread, sprinkler activation) over a wide range of grid sizes.
³³ In general, fire modelling is rather challenging, not only due to the different physical processes that
³⁴ need to be considered (i.e., turbulence, combustion, radiation, soot, heat transfer) but also due to the
³⁵ wide range of length and time scales involved. Within this framework, combustion is an important
³⁶ modelling aspect, strongly coupled to turbulence and radiation modelling, which requires special
³⁷ attention. This is particularly important for accurate prediction of the fuel gasification rate (i.e.,

either pyrolysis or liquid evaporation) as it is determined by a heat feedback mechanism which strongly depends on combustion and (convective / radiative) heat transfer. The current state-of-the-art approach of combustion modelling in the context of fires relies on the use of infinitely fast chemistry. Considering that the chemical time scales are much smaller than the flow time scales (i.e., $Da \gg 1$), chemical reactions are then limited by the turbulent mixing between fuel and oxidizer occurring on a sub-grid scale level. This approach has proven to be fairly accurate for a wide range of different fire scenarios (e.g., [1, 2]) without the need to employ more advanced combustion models (e.g., considering finite rate chemistry). Nevertheless, fire simulations still strongly rely on the use of models (e.g., Eddy Dissipation Model (EDM) [8]) and their corresponding parameters have been developed for combustion applications, where the flow conditions are significantly different from those encountered in fires (i.e., momentum-driven versus buoyancy-driven flows with different Reynolds numbers). Some notable examples involving the use of the EDM combustion model in fire research include [9, 10, 11, 12, 13].

The paper focuses on Large Eddy Simulations (LES) and combustion modelling using infinitely fast chemistry and aims to investigate the impact of the sub-grid scale micro-mixing model in the context of fire modelling. The motivation for performing the work presented in the paper relates to flame extinction and re-ignition modelling. Within the context of fires, with the use of infinitely fast chemistry, modelling of flame extinction often relies on the concept of a critical flame temperature while re-ignition relies on the use of a constant re-ignition temperature. Therefore, in such scenarios, accurate results for the flame temperatures, over a wide range of grid sizes, is of great importance for predicting e.g., the limiting oxygen concentrations at extinction. Differences in the predicted flame temperatures can potentially lead to discrepancies in the predictions of flame extinction. The effect of sub-grid scale (sgs) micro-mixing has been extensively studied within the combustion community in the past (e.g., [3, 4, 5]) but has received less attention within the fire community. A set of three experimental test cases from the MaCFP workshop [1] (i.e., McCaffrey's fire plumes, UMD line burner and NIST pool fire), involving different burners geometries, fire sizes and fuel types, are considered for validation purposes of the CFD simulations.

2. Numerical modelling

The CFD code FireFOAM, solving the Navier-Stokes equations along with transport equations for species mass fractions and sensible enthalpy, is employed. An overview of the governing equations that are used in the code has been previously reported in [2].

2.1 Turbulence

The dynamic Smagorinsky model [6] is used for turbulence, calculating the sgs viscosity as:

$$\mu_{sgs} = \bar{\rho}(c_s \Delta)^2 |\tilde{S}| \quad (1)$$

where Δ is the filter width (i.e., cube root of the cell volume) and \tilde{S} is the (resolved) strain rate.

The sub-grid kinetic energy is estimated as [7]:

$$k_{sgs} = c_I \Delta^2 |\tilde{S}|^2 \quad (2)$$

73 The sub-grid scale dissipation rate is estimated as [7]:

$$\epsilon_{sgs} = \frac{c_\epsilon k_{sgs}^{3/2}}{\Delta} \quad (3)$$

74 where $c_\epsilon = 1.0$ [7] is a model constant.

75 A dynamic procedure is employed for the calculation of the model parameters, c_s , c_I , as well as for
76 the turbulent Prandtl number, Pr_t , which has been previously reported in [2]. A dynamic calculation
77 of c_ϵ will be considered in the future.

78 2.2 Combustion

79 The combustion model considers a one-step, infinitely fast, irreversible chemical reaction combined
80 with the eddy dissipation model [8] for modelling turbulence-chemistry interactions. The EDM
81 model calculates the fuel reaction rate as:

$$\overline{\dot{\omega}_F''' = -\bar{\rho} \frac{\min(\tilde{Y}_F, \tilde{Y}_{O_2}/s)}{\tau_{mix}}} \quad (4)$$

82 where \tilde{Y}_F and \tilde{Y}_{O_2} are the fuel and oxygen mass fractions, respectively and s is the stoichiometric
83 oxygen-to-fuel ratio.

84 The EDM model considers chemical reactions to be infinitely fast and combustion to be governed
85 by turbulent mixing, hence, a turbulent mixing time is used for the calculation of the fuel reactions
86 rate. Within the context of LES, mixing is considered to be a sgs phenomenon, not fully resolved
87 by the grid size. It is common practice to use sgs quantities to determine the mixing time scale.
88 Nevertheless, determination of the appropriate mixing time scale is not straightforward as there
89 is a wide range of time scales (e.g., associated with diffusive, advective and/or buoyant transport)
90 typically involved in fire scenarios. Here, turbulent mixing is assumed to be governed mainly by
91 sgs advection/diffusion and can be described in terms of sub-grid scale quantities. For this reason,
92 six different approaches for estimating the mixing time scale, τ_{mix} , on a sub-grid scale level are
93 considered and are presented in detail below. To avoid confusion, all the reported mixing time
94 scale models below have been evaluated at a sub-grid scale (sgs) level. Hence, the term ‘Integral’
95 will refer to the largest turbulent time scale at a sgs level and should not be confused with the
96 characteristic integral (largest) time scales of turbulence.

- 97 • Model 1 (i.e., named ‘Global-A’): This approach considers the default time scale of EDM [8]
98 which is calculated as a fraction of the integral time scale, k_{sgs}/ϵ_{sgs} , as:

$$\tau_{mix, Global-A} = \frac{k_{sgs}}{A \epsilon_{sgs}} \quad (5)$$

99 where $A = 4$ [8] is a model parameter, calibrated based on turbulent premixed and diffusion
100 flames and essentially incorporating the chemistry effects that are neglected by the model.

- 101 • Model 2 (i.e., named ‘Local-A’): The mixing time scale is calculated as a fraction of the
 102 integral time scale, k_{sgs}/ϵ_{sgs} , (i.e., similarly as in EDM [8]) as:

$$\tau_{mix, Local-A} = \frac{k_{sgs}}{A\epsilon_{sgs}} \quad (6)$$

103 but with A now varying in space and time as a function of the standard deviation of the
 104 mixture fraction \tilde{z}' , considering a clipped Gaussian shape for the mixture fraction from the
 105 theoretical analysis of Brizuela & Bilger [14].

106 The mixture fraction, \tilde{z} , is calculated as:

$$\tilde{z} = \frac{s\tilde{Y}_F - \tilde{Y}_{O_2} + Y_{O_2,0}}{sY_{F,0} + Y_{O_2,0}} \quad (7)$$

107 where $Y_{F,0}$ is the fuel mass fraction in the fuel stream (i.e., 1) and $Y_{O_2,0}$ is the oxygen mass
 108 fraction in the oxidizer stream (i.e., 0.233).

109 The mixture fraction variance, \tilde{z}''^2 , is calculated considering a scale similarity model as [15]:

$$\tilde{z}''^2 = c_z \Delta^2 (\nabla \tilde{z})^2 \quad (8)$$

110 where $c_z = 0.1$ [16] is a model constant. A dynamic calculation of c_z was found to require
 111 clipping on its lower value, which affected the model performance, hence was not employed
 112 here. The standard deviation of the mixture fraction, \tilde{z}' , is then approximated as $\tilde{z}' \equiv (\tilde{z}''^2)^{1/2}$.

113 The stoichiometric mixture fraction, z_{st} , is:

$$z_{st} = \frac{1}{1+r} \quad (9)$$

114 where r is the stoichiometric air-to-fuel ratio.

115 The EDM model parameter, A , is then calculated as:

$$A = 2.0037 - 0.5426 \left(\frac{\tilde{z}'}{z_{st}} \right) + 0.2065 \left(\frac{\tilde{z}'}{z_{st}} \right)^2 \quad (10)$$

116 considering a second degree polynomial fit (i.e., $R^2 = 0.94$) of the average A values as a
 117 function of the standard deviation of the mixture fraction (i.e., using a clipped Gaussian pdf)
 118 from the theoretical analysis of Brizuela & Bilger [14]. Based on the fitting equation, $A \approx 2$
 119 for $\tilde{z}'/z_{st} < 2$, which is half the value used in the standard EDM model. Values of $A = 2$
 120 will be fairly accurate in the rich flame region but may overestimate or underestimate A by
 121 a factor of two from the lean side to approximately $2z_{st}$, and will underestimate A by one to
 122 two orders of magnitude in the rich region (i.e., beyond $2z_{st}$) [14]. To the best of the authors’
 123 knowledge, has never been considered in the literature in the past.

- 124 • Model 3 (i.e., named ‘Mean’): This approach considers only the two most important turbulent
 125 time scales; the integral time scale (i.e., k_{sgs}/ϵ_{sgs}), associated with large-scale mixing, and
 126 the Kolmogorov time scale (i.e., $(\nu/\epsilon_{sgs})^{1/2}$), associated with the mixing on molecular level.

127 It has been proposed that the easiest way to account for both these important turbulent time
 128 scales in the mixing process is through the use of a synthetic time scale, calculated based on
 129 their geometric mean as [19]:

$$\tau_{mix, Mean} = \sqrt{\frac{k_{sgs}}{\epsilon_{sgs}} \left(\frac{\nu}{\epsilon_{sgs}} \right)^{1/2}} \quad (11)$$

- 130 • Model 4 (i.e., named ‘Mean-LES’): In the context of LES, an alternative synthetic mixing
 131 time scale can be calculated based on the geometric mean of the sub-grid velocity stretching
 132 time scale (i.e., Δ/u') and the Kolmogorov time scale (i.e., $(\nu/\epsilon_{sgs})^{1/2}$) as [20]:

$$\tau_{mix, Mean-LES} = \sqrt{\frac{\Delta}{u'} \left(\frac{\nu}{\epsilon_{sgs}} \right)^{1/2}} \quad (12)$$

133 where $u' = (2k_{sgs}/3)^{1/2}$ is the rms of the sgs turbulent velocity fluctuations. It should be
 134 noted that models 3 and 4 essentially only differ by a proportionality constant. Their behavior
 135 is similar for $c_\epsilon = 1.0$, however they will deviate with lower c_ϵ values, as a function of Re_t .

- 136 • Model 5 (i.e., named ‘Diffusion’): The mixing time scale is based on the local variation
 137 of the scalar dissipation rate, $\tilde{\chi}$, and the mixture fraction variance, $\tilde{z''^2}$. Considering local
 138 equilibrium (i.e., production equals dissipation rate in the scalar variance equation), the scalar
 139 dissipation rate is estimated based on an algebraic equilibrium model [21]:

$$\tilde{\chi} = 2(D + D_{sgs})(\nabla \tilde{z})^2 \quad (13)$$

140 while the mixture fraction variance, $\tilde{z''^2}$, is estimated based on the scale similarity model
 141 previously presented in the ‘Local-A’ approach (i.e., Eq. (8)).

142 A mixing time scale can then be calculated as [22]:

$$\tau_{mix, Diffusion} = \frac{\tilde{z''^2}}{\tilde{\chi}} = \frac{c_z \Delta^2}{2(D + D_{sgs})} \quad (14)$$

143 where $c_z = 0.1$ [16]. The resulting expression can be considered as an effective diffusion time
 144 scale (i.e., considering both molecular and sgs diffusive transport). In addition, the mixing
 145 time scale does not explicitly depend on the sub-grid scale dissipation rate ϵ_{sgs} .

- 146 • Model 6 (i.e., named ‘FDS’): The model, which is used in the Fire Dynamics Simulator (FDS)
 147 code, compares the mixing times for diffusion (i.e., τ_d), sub-grid scale advection (i.e., τ_u),
 148 and buoyant acceleration (i.e., τ_g) and is expressed as [17]:

$$\tau_{mix, FDS} = \min(\tau_d, \tau_u, \tau_g) \quad (15)$$

149 with $\tau_d = \frac{\Delta^2}{D_F}$, $\tau_u = \frac{C_u \Delta}{\sqrt{(2/3)k_{sgs}}}$, and $\tau_g = \sqrt{\frac{2\Delta}{g}}$ where D_F is the effective diffusivity of the fuel
 150 and $C_u = 0.4$ is a model parameter calibrated to match Heskestad’s flame height correlation.

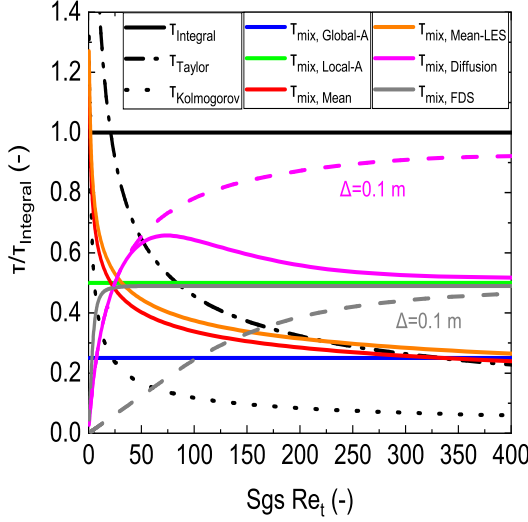


Fig. 1. Comparison of the different normalised time scales for a grid size of $\Delta = 0.01$ m as a function of the sgs turbulent Reynolds number, Re_t . The dashed lines correspond to $\Delta = 0.1$ m.

151 A comparison between the different normalised time scales, $\tau/\tau_{Integral}$, as a function of the sgs
 152 turbulent Reynolds number, $Re_t = k_{sgs}^2/(\nu\epsilon_{sgs})$, is presented in Figure 1. For the purpose of the
 153 analysis, a grid size of $\Delta = 0.01$ m, a kinematic viscosity of $\nu = 17.41 \times 10^{-5}$ m²/s, based on an
 154 average flame temperature of 1000°C, and a constant value of $A = 2$ for $\tau_{mix, Local-A}$ have been
 155 employed. The sgs kinematic viscosity is evaluated as $\nu_{sgs} = c_k \Delta \sqrt{k}$ with $c_k = 0.05$ (i.e., equivalent
 156 Smagorinsky constant of $c_s \approx 0.1$) for $Re_t \leq 100$ and $c_k = 0.094$ (i.e., equivalent Smagorinsky
 157 constant of $c_s \approx 0.17$) for $Re_t > 100$ (i.e., increasing c_k values with increasing turbulence). In this
 158 case, low Re_t values have been considered, similar to the values reported by Weckman et al. [26]
 159 in the near-field region of a 21.3 kW methanol pool fire, which are consistent with buoyancy-driven
 160 turbulent flows. The values for $\tau_{mix, Global-A}$ and $\tau_{mix, Local-A}$, in this case, are straight lines at
 161 0.25 and 0.5, respectively. For low sgs turbulent Reynolds values (i.e., $1 < Re_t < 25$), where
 162 the flow is typically only weakly turbulent and molecular effects can start becoming important, all
 163 mixing time scales tend towards the Kolmogorov time scale. Nevertheless, the limiting behaviour
 164 is somewhat different with $\tau_{mix, Mean}$ and $\tau_{mix, Mean-LES}$ exhibiting an asymptotical behaviour
 165 towards $\tau_{Kolmogorov}$ while $\tau_{mix, Diffusion}$ and $\tau_{mix, FDS}$ converge to a finite value (i.e., $\frac{0.1\Delta^2}{2\nu}$ and
 166 $\sqrt{\frac{2\Delta}{g}}$, respectively). With increasing sgs turbulent Reynolds number (i.e., $25 < Re_t < 100$),
 167 most time scales lie approximately between the Kolmogorov and the Taylor time scales. For sgs
 168 turbulent Reynolds numbers $Re_t > 300$, $\tau_{mix, Global-A}$, $\tau_{mix, Mean}$ and $\tau_{mix, Mean-LES}$ converge
 169 towards the Taylor time scale (i.e., $(15\nu/\epsilon_{sgs})^{1/2}$) while $\tau_{mix, Diffusion}$ and $\tau_{mix, FDS}$ converge
 170 towards $\tau_{mix, local-A}$ (i.e., to a value equal to half the integral time scale). Note that the grid size
 171 will have a more direct impact in the ‘Diffusion’ and the ‘FDS’ models, as opposed to the other
 172 time scale models, as Δ is explicitly used in the calculation of $\tau_{Diffusion}$ and τ_g , respectively.
 173 Increasing Δ values result in higher $\tau_{Diffusion}$ values (i.e., slower mixing) and lower τ_{FDS} values
 174 (i.e., faster mixing). This different behaviour with respect to Δ will be important on coarse-grid
 175 simulations. The mixing time for all models scales with $1/S \sim \Delta^{2/3}$ in the inertial sub-range.
 176 The limiting behaviour when $\Delta \rightarrow 0$ is different between the models, though: models 5 and 6 go

¹⁷⁷ towards a molecular diffusion mixing time while models 1 - 4 will have to be limited by a laminar
¹⁷⁸ mixing time. The various mixing models can be grouped as advection-controlled (models 1-4),
¹⁷⁹ diffusion-controlled (model 5) and mixed (model 6).

¹⁸⁰ **2.3 Radiation**

¹⁸¹ The radiation modelling approach employed considers the radiative intensity to be a function of
¹⁸² both spatial location and angular direction and is obtained by solving the radiative transfer equation
¹⁸³ (RTE) using the finite volume discrete ordinates model. Assuming a non-absorbing and optically
¹⁸⁴ thin medium, the radiative heat fluxes are calculated as:

$$\nabla \cdot \overline{\dot{q}_r''} = \chi_r \overline{\dot{q}_c'''} \quad (16)$$

¹⁸⁵ where χ_r is the radiative fraction of the fuel. This approach does not require any turbulence-radiation
¹⁸⁶ interactions (TRI) modelling, which could potentially be important on coarse grids. In addition,
¹⁸⁷ the employed approach guarantees that the correct amount of heat will be 'lost' per unit time due
¹⁸⁸ to radiation so that the evaluation of the various micro-mixing models can be done independent of
¹⁸⁹ any uncertainties related to radiation modelling.

¹⁹⁰ **3. Experimental test cases**

¹⁹¹ The experiments considered for model validation are target cases of the MaCFP workshop series
¹⁹² [1] and a detailed description is already available (i.e., <https://github.com/MaCFP>), hence, only
¹⁹³ a brief overview is outlined here. All cases involve buoyancy-driven flows with non-sooty fuels
¹⁹⁴ in order to avoid uncertainties related to soot modelling and cover both medium and large scale
¹⁹⁵ fires. The first case is McCaffrey's fire plume experiments [24] which consist of a 30 cm square
¹⁹⁶ burner, raised 75 cm from the ground, with natural gas as fuel and heat release rates of 14.4 -
¹⁹⁷ 57.5 kW. The second case is the UMD line burner experiments [25] which consist of a low-strain,
¹⁹⁸ buoyancy-driven, fully-turbulent methane diffusion flame in a canonical line-fire configuration. The
¹⁹⁹ burner measures 5 cm wide by 50 cm long with the fuel mass flow rate set to 1 g/s (i.e., 50 kW)
²⁰⁰ while the co-flowing oxidizer (i.e., air) is issued at 85 g/s. The third case is the NIST experiments
²⁰¹ [27] involving a circular steel pan with an inner diameter of 1 m, raised 30 cm above the floor. The
²⁰² liquid fuel is methanol with a measured heat release rate of 256 kW.

²⁰³ **4. Numerical setup**

²⁰⁴ An overview of the most important modelling parameters (e.g., computational domain, grid size,
²⁰⁵ total number of cells) considered in the simulations is outlined in Table 1. A local grid refinement
²⁰⁶ strategy is employed for all cases (see Figure 2) ensuring good grid resolution in the near-field
²⁰⁷ region of the fire plumes (i.e., the grid refinement extends above the experimentally reported flame
²⁰⁸ heights). Based on the grid requirements [1] needed for accurate resolution of the fire plume
²⁰⁹ dynamics, the finest grid sizes used to simulate the cases are in the order of 1 cm or less. Such grid
²¹⁰ sizes, previously proven accurate based on grid refinement studies for the same test cases [2], also
²¹¹ make sure that the ratio of the characteristic fire size, $D^* = \left(\frac{\dot{Q}}{\rho_\infty c_p T_\infty \sqrt{g}}\right)^{2/5}$, to the grid size, Δ , is
²¹² in the order of 10 - 15 or higher [1]. The ambient temperature and pressure are set to 293 K and

Table 1. Overview of the setup used in the numerical simulations.

Case	McCaffrey's fire plumes [24]	UMD line burner [25]	NIST pool fire [27]
Fuel	CH ₄	CH ₄	CH ₃ OH
HRR (\dot{Q})	14.4, 21.7, 33, 44.9, 57.5 kW	50 kW	256 kW
Burner dimensions	0.3 m x 0.3 m (square)	0.5 m x 0.05 m (line)	1 m diameter (circular)
Domain	3 m x 3.3 m x 3 m (rectangular)	1.6 m x 2 m x 1 m (rectangular)	4 m x 4 m (cylindrical)
Grid size (Δ)	1.5 cm (1 m x 2.3 m x 1 m) 3 cm (2 m x 3.3 m x 2 m) 6 cm (domain)	0.625 cm (0.6 m x 0.6 m x 0.4 m) 1.25 cm (0.8 m x 0.8 m x 0.6 m) 2.5 cm (domain)	1 cm (1.5 m x 1.5 m) 2 cm (2.5 m x 2.5 m) 4 cm, 8 cm (domain)
D^*/Δ	12 - 20	-	55
Cells	1.2 million	0.89 million	1.99 million
Rad. fraction (χ_r)	0.17, 0.21, 0.25, 0.27, 0.27	0.24	0.21

213 101325 Pa, respectively. The mass flow rate is applied at the inlet (accounting for both convective
 214 and diffusive mass fluxes), calculated based on the corresponding heat release rate and the heat of
 215 combustion of the fuel. The equations are advanced in time using a second order backward scheme.
 216 For the convective terms, a second order filtered linear scheme (filteredLinear2V) is used. A TVD
 217 scheme (limitedLinear) is employed for scalar transport while a central difference scheme for the
 218 diffusive terms. The choice of the numerical schemes is based on [28]. For the solution of the
 219 radiative transfer equation, 72 solid angles are used for angular discretization. The running time for
 220 all simulations is set to 35 s using a varying time step, limited by a maximum Courant number of
 221 0.9, with averaging occurring over the last 30 s.

222 5. Results

223 5.1 McCaffrey's fire plumes

224 The CFD predictions for McCaffrey's fire plumes are presented in Figures 3 - 5 together with the
 225 empirical correlations (i.e., black dashed lines) for the centerline excess temperature. The scaling
 226 of temperature is fairly good for all models on the finest grid size (i.e., 1.5 cm) as shown in Figure 3
 227 and the predictions remain close to empirical correlation, apart from 'Diffusion', for which the
 228 clustering of data in the intermittent (i.e., $0.08 < y/\dot{Q}^{2/5} < 0.2$) and plume (i.e., $y/\dot{Q}^{2/5} > 0.2$)
 229 regions is less satisfactory. The discrepancies are particularly obvious for the lower HRR cases (i.e.,
 230 14.4 - 33 kW) which also exhibit lower levels of turbulence, compared to the higher HRR cases
 231 (i.e., 44.9 - 57.5 kW), and could be attributed to the longer mixing times predicted by the model

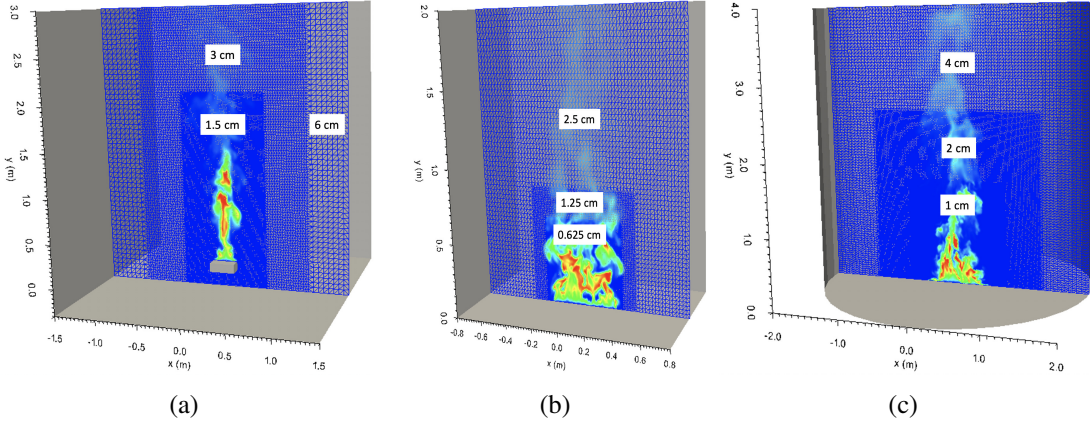


Fig. 2. Computational domain and local grid refinement used for the (a) McCaffrey's fire plumes, (b) UMD line burner and (c) NIST pool fire.

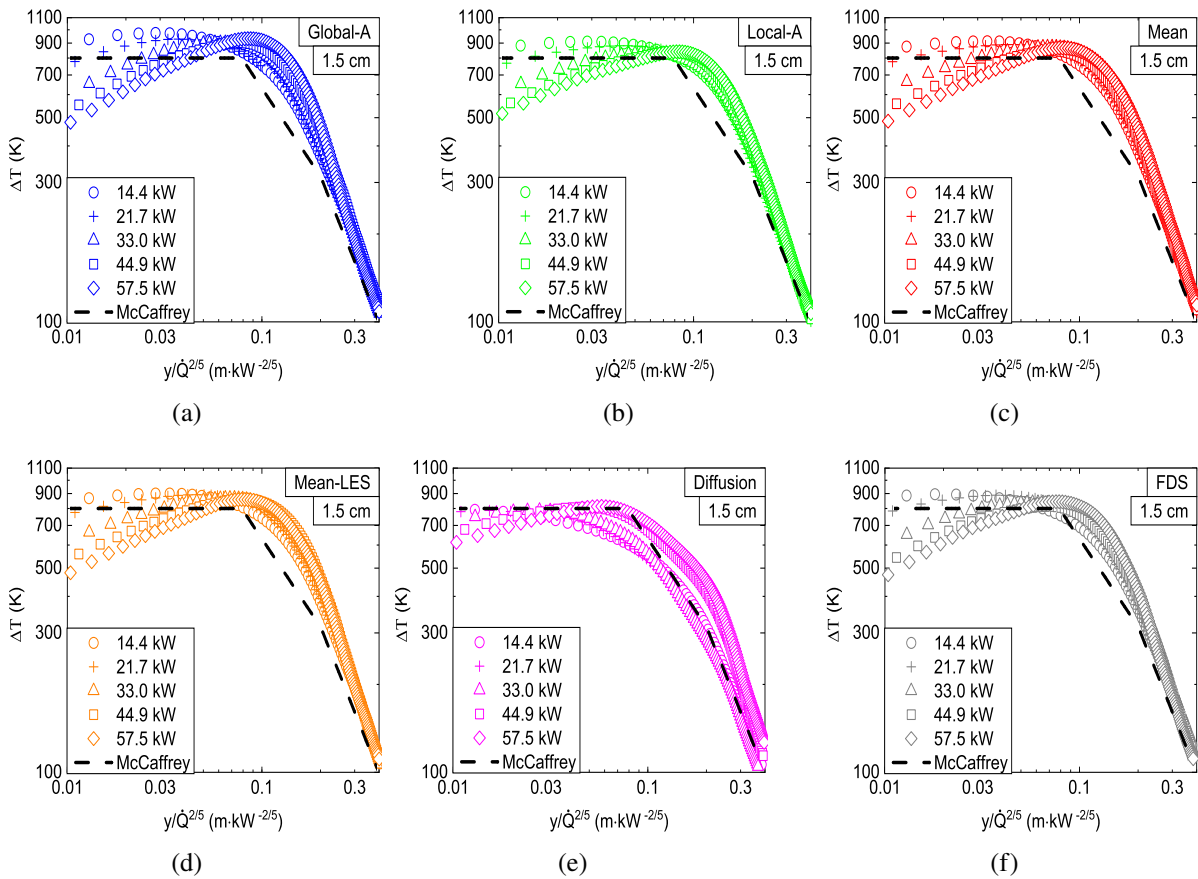


Fig. 3. Centerline excess temperature with (a) 'Global-A', (b) 'Local-A', (c) 'Mean', (d) 'Mean-LES', (e) 'Diffusion' and (f) 'FDS' with a 1.5 cm grid size for McCaffrey's plumes.

for moderately low sgs Re_t values (i.e., $25 < Re_t < 100$ region in Figure 1). Overall, the absolute values of temperature are similar for all models, apart from the predictions of 'Global-A' in the

flame and intermittent regions, which are 50 - 100 K higher for certain scenarios (e.g., for the 14.4 kW case in the flame region, for the 57.5 kW case in the intermittent region). Interestingly enough, the scaling of temperature remains acceptable for all models, apart from ‘Diffusion’, even on the coarser grid size of 3 cm (i.e., 10 cells across the burner diameter) which is very encouraging with respect to the employed dynamic modelling approach. On the other hand, the grid size of 6 cm (i.e., only 5 cells across the burner diameter) can be considered too coarse, even for engineering type of calculations: it does not result in good scaling for the considered range of heat release rates with any of the models. A notable exception is the highest heat release rate cases (i.e., 57.5 kW), for which the predictions still remain fairly reasonable indicating that coarser grid sizes can be used with higher heat release rate fires (i.e., bigger Q^* values for the same grid size for increasing heat release rate). In this case, ‘Diffusion’ totally fails to predict any sort of scaling and the temperatures remain excessively low. The reason for this behaviour is the low levels of turbulence above the burner when coarser grids are employed, resulting in zero sub-grid scale quantities (e.g., ν_{sgs}) predicted from the turbulence model. When this occurs, the computed mixing times with ‘Diffusion’ (see Equation (14)) only rely on the molecular kinematic viscosity (i.e., ν) and result in fairly long mixing times, hence, low reaction rates. It is worth noting that this behaviour with ‘Diffusion’ on very coarse grids (i.e., zero sgs values above the burner) would not be present if static turbulence models were employed. However, a static model would then be unable to correctly predict the laminar to turbulent transition typically occurring above fire sources and would potentially require some model calibration in order to get the correct scaling. Furthermore, it is reasonable to assume that the consideration of multiple time scales would be beneficial for describing mixing more accurately, as a function of different grid sizes, compared to other models which only consider a single time scale. In fact, such a scenario is considered with the use of ‘FDS’ in the simulations. Interestingly enough, the behaviour of ‘FDS’ in this scenario is very similar to ‘Local-A’ , ‘Mean’ and ‘Mean-LES’ and does not exhibit any particular advantages compared to the other models.

5.2 UMD line burner

Figure 6 presents the predicted mean and rms centerline temperatures, as a function of grid size, for the UMD line burner case. The predictions of all mixing models on the finest grid size considered (i.e., 0.625 cm) follow the experimental profiles fairly well and in most cases remain close to the experimental uncertainty. The CFD predictions (i.e., in terms of maximum flame temperature, location of the maximum flame temperature and temperature decay on the centerline) on the coarser grid size of 1.25 cm remain good for all models, apart from ‘Diffusion’, which fails to accurately predict the maximum flame temperatures by 100 - 150 K. The simulations on the coarsest grid size (i.e., 2.5 cm) still manage to accurately predict both the location and the absolute value of the maximum flame temperature, but do not capture well the decay of temperature on the centerline. Overall, the main differences between the various micro-mixing models remain limited around the location of the maximum flame temperature (i.e., in the flame region) with the highest temperatures consistently obtained with ‘Global-A’ for all grid sizes. The computed sgs turbulent Reynolds numbers from the simulations on the finest grid size considered (i.e., 0.625 cm) were in the order of $Re_t < 25$ up to the experimentally reported flame height (approximately 0.5 m). In this low turbulence region in Figure 1, $\tau_{mix, Global-A}$ has the shortest mixing times, compared to the other models, which explains the highest temperatures obtained. In general, the predictions of ‘Diffusion’, even though accurate on the finest grid size employed, reveal that the model is highly grid-sensitive

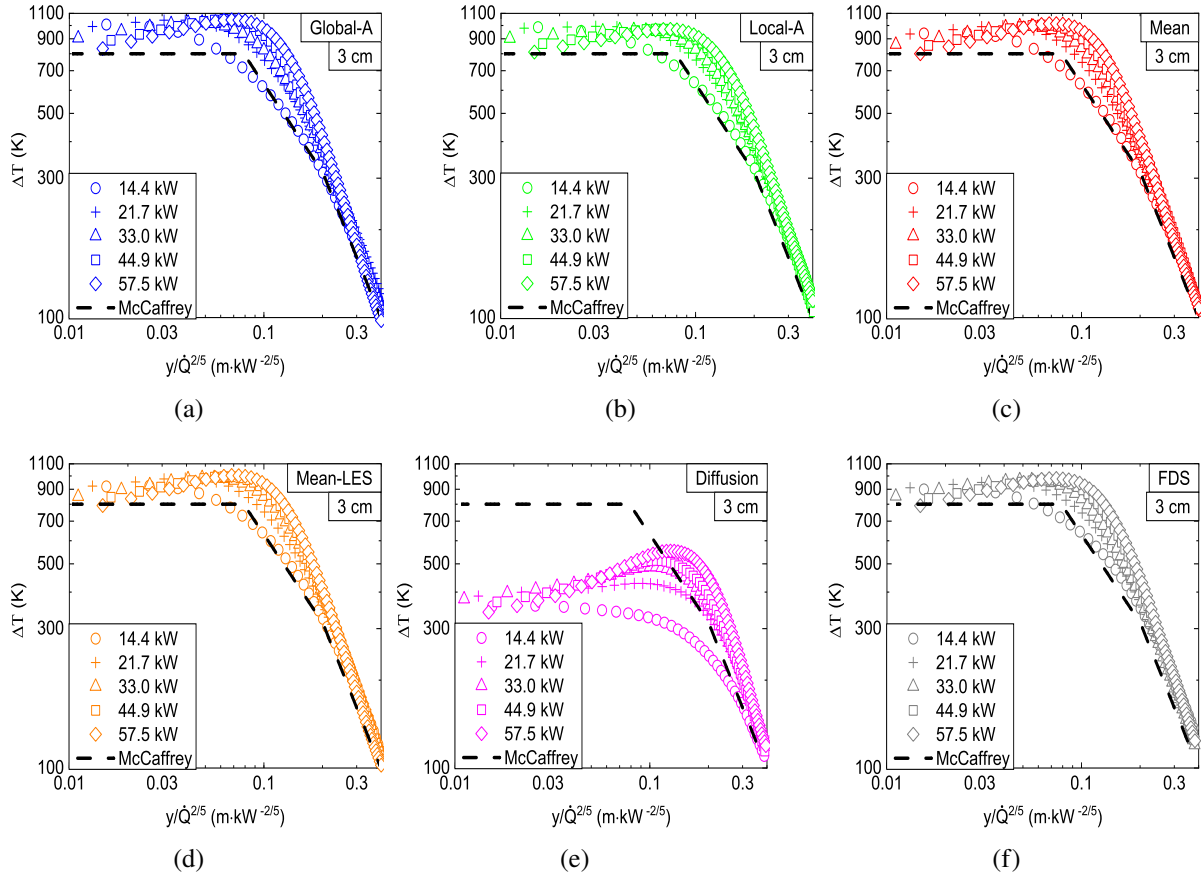


Fig. 4. Centerline excess temperature with (a) ‘Global-A’, (b) ‘Local-A’, (c) ‘Mean’, (d) ‘Mean-LES’, (e) ‘Diffusion’ and (f) ‘FDS’ with a 3 cm grid size for McCaffrey’s plumes.

and not suitable for coarse grid simulations with the use of dynamic turbulence models in the context of fires. No significant differences are evident in the predicted rms temperatures for all models as a function of grid size and the results remain within the experimental uncertainty in most axial locations examined. Some discrepancies (i.e., under-predicted values) are evident for heights up to $y < 0.1$ m when coarser grid sizes are considered (i.e., 1.25 - 2.5 cm) indicating that the fire plumes are not turbulent enough very close to the burner. This outcome is not surprising as there are only 4 and 2 cells, respectively, across the width of the burner in these cases. Still, even on such coarse grids, the employed approach is able to predict the fire plume dynamics in a fairly accurate way.

5.3 NIST pool fire

Figure 7 presents the predicted centerline mean and rms temperatures with the different sub-grid scale mixing models versus the axial distance normalised by $\dot{Q}^{2/5}$ for the NIST pool fire case. In addition, experimental data of 30 cm in diameter methanol pool fires are included for comparison purposes. The maximum temperature is well captured by all models and the predictions remain close to the experimental uncertainty on the finer grid sizes considered (i.e., 1 - 2 cm). The predictions on the coarser grid size (i.e., 4 cm) are still in good agreement with the experiments for all models, apart from ‘Diffusion’ which significantly under-predict the maximum flame temperature. The

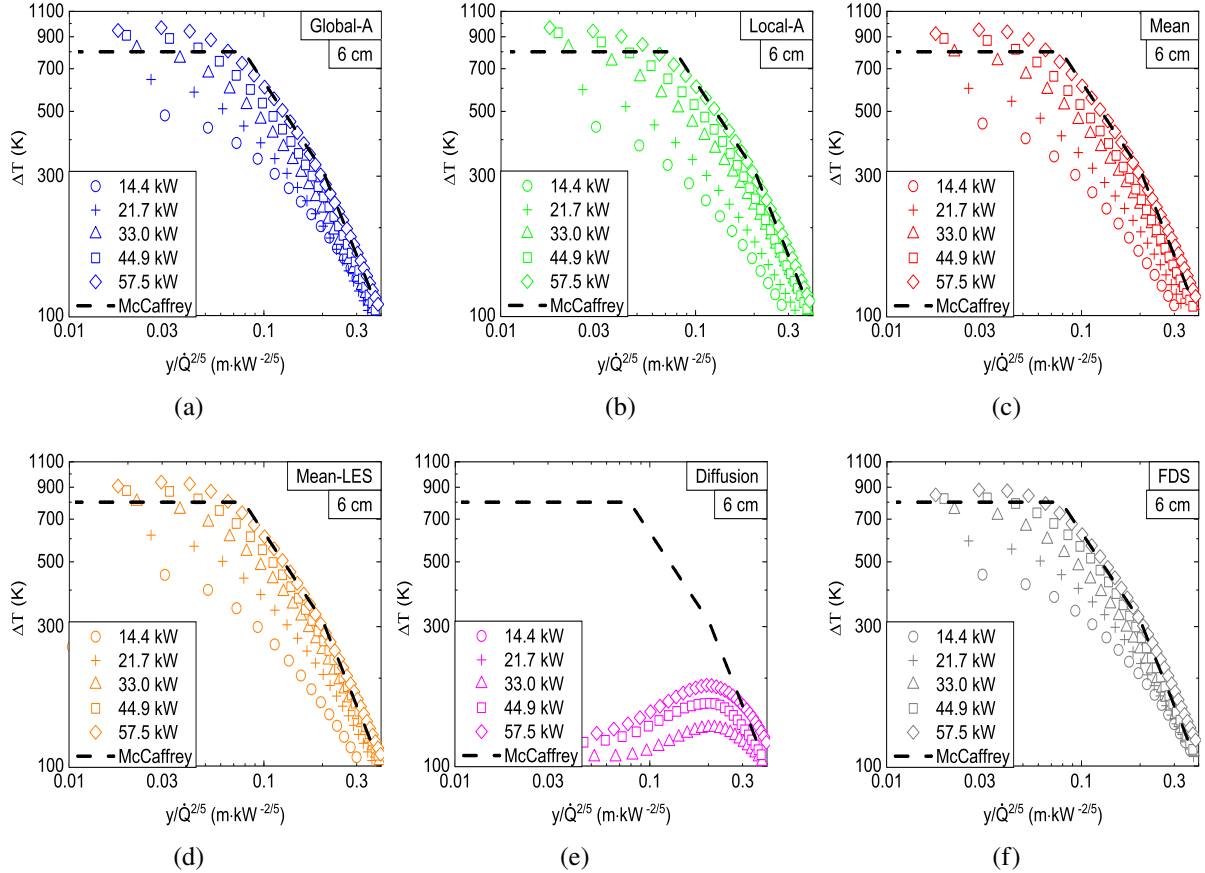


Fig. 5. Centerline excess temperature with (a) ‘Global-A’, (b) ‘Local-A’, (c) ‘Mean’, (d) ‘Mean-LES’, (e) ‘Diffusion’ and (f) ‘FDS’ with a 6 cm grid size for McCaffrey’s plumes.

simulation results on the coarsest grid size (i.e., 8 cm), however, do exhibit some differences between the various models. The predictions of ‘Local-A’ and ‘FDS’ are similar, and within the experimental uncertainty, while the predictions of ‘Global-A’, ‘Mean’ and ‘Mean-LES’ significantly over-predict the maximum flame temperature by approximately 300 K. From Figure 1 it can be seen that the mixing time of ‘FDS’, on similarly coarse grids (i.e., $\Delta = 0.1$ m), tends towards ‘Local-A’ with increasing sgs Re_t values. The NIST pool fire scenario, involves a fire source which is larger in diameter compared to the previous cases, hence, it will be more turbulence and result in higher sgs turbulent Reynolds number values. Therefore, it is not surprising that the predictions of both these models are similar. On the other hand, for the same sgs turbulent Reynolds number value (with $Re_t > 25$), the mixing time scales of ‘Global-A’, ‘Mean’ and ‘Mean-LES’ are shorter, hence, result in faster reaction rates and higher flame temperatures. The poor behaviour of ‘Diffusion’ can also be explained from Figure 1 as the mixing time of the model increases (i.e., slower reaction) for coarser grid sizes. Some discrepancies are evident around the location of the experimentally reported flame height (i.e., 1.1 m [27] or $y/\dot{Q}^{2/5} \approx 0.12$) where the rms temperatures are over-predicted for all models. Part of the discrepancies could perhaps be attributed to radiation modelling: the use of the radiative fraction approach, ignoring absorption, perhaps becomes less valid in large-scale fires.

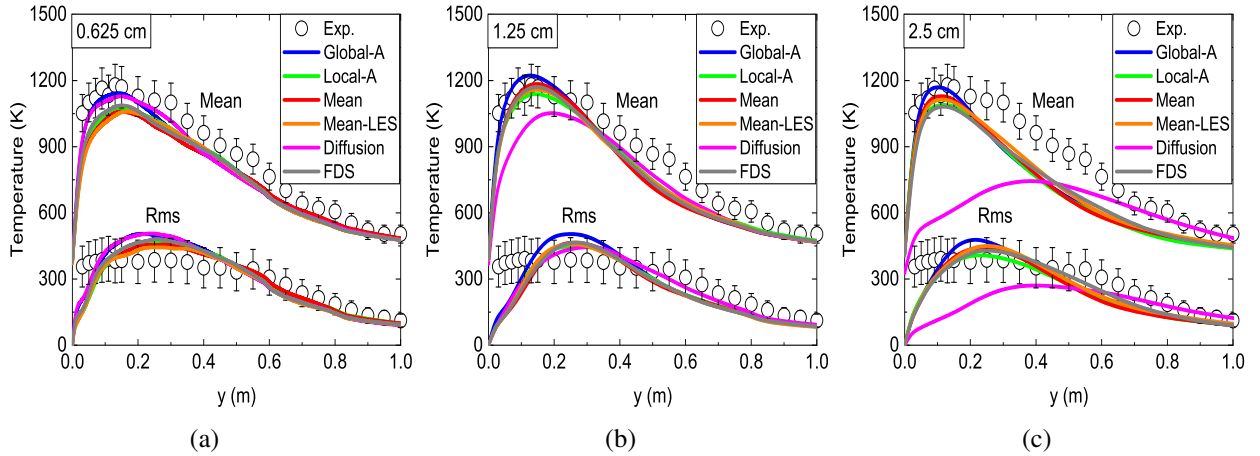


Fig. 6. Centerline mean and rms temperatures using different micro-mixing models with a grid size of (a) 0.625 cm, (b) 1.25 cm and (c) 2.5 cm for the UMD line burner.

5.4 Discussion

Fires typically involve much lower scalar dissipation rates compared to jet flames. There are also significant differences between jet flames (i.e., momentum-driven flows) and fires (i.e., buoyancy-driven flows) in terms of mixing, entrainment characteristics as well as of the impact of buoyancy and radiation. Based on these significant differences, validation of a mixing time scale model in jet flame scenarios will not necessarily lead to a good performance in fire scenarios as well. This is actually the case as it is illustrated in the paper (e.g., with the ‘Diffusion’ mixing time scale model). In many fire scenarios, the flow conditions just above the fire source are not highly turbulent and it usually takes some axial distance from the source (i.e., in the order of an inlet diameter) until turbulence starts to increase due to buoyancy. This effect is even more pronounced when coarse grids are used in the simulations. In such scenarios and in regions just above the fire source, dynamic turbulence models will typically predict negative (which are clipped to zero) / low values for the sgs viscosity (and mass diffusivity), contrary to the values of the sgs kinetic energy which are non-zero and significantly higher. This is the typically the region where the so-called reverse energy cascade occurs (i.e., transfer of energy from the small to the large scales).

Coarse-grid simulations typically involve higher sgs Re_t values while finer-grid simulations have lower sgs Re_t values. The similar model performance observed on coarse grids (e.g., $\Delta > 6$ cm) for ‘FDS’ and ‘Local-A’ occurs in regions where $Re_t > 300$ and their mixing times are similar. In addition, the centerline variation (i.e., across z/L_f where L_f is the flame height) of A using the finest grid sizes in the different cases is presented in Figure 8. The resulting average A values with ‘Local-A’ (i.e., Eq. (10)) were around 2 and only slightly varied (up to $\pm 15\%$) in axial locations very close to the burner. This implies that, as also reported in Figure 1, in many instances ‘FDS’ and ‘Local-A’ performed similarly.

An improvement of the performance of the models (where applicable), particularly on coarser grids, could potentially be made with the use of a dynamic model for the determination of c_ϵ in the calculation of the sgs dissipation rate, ϵ_{sgs} . In addition, a laminar time scale (i.e., $\tau_{lam} = \Delta^2/D$)

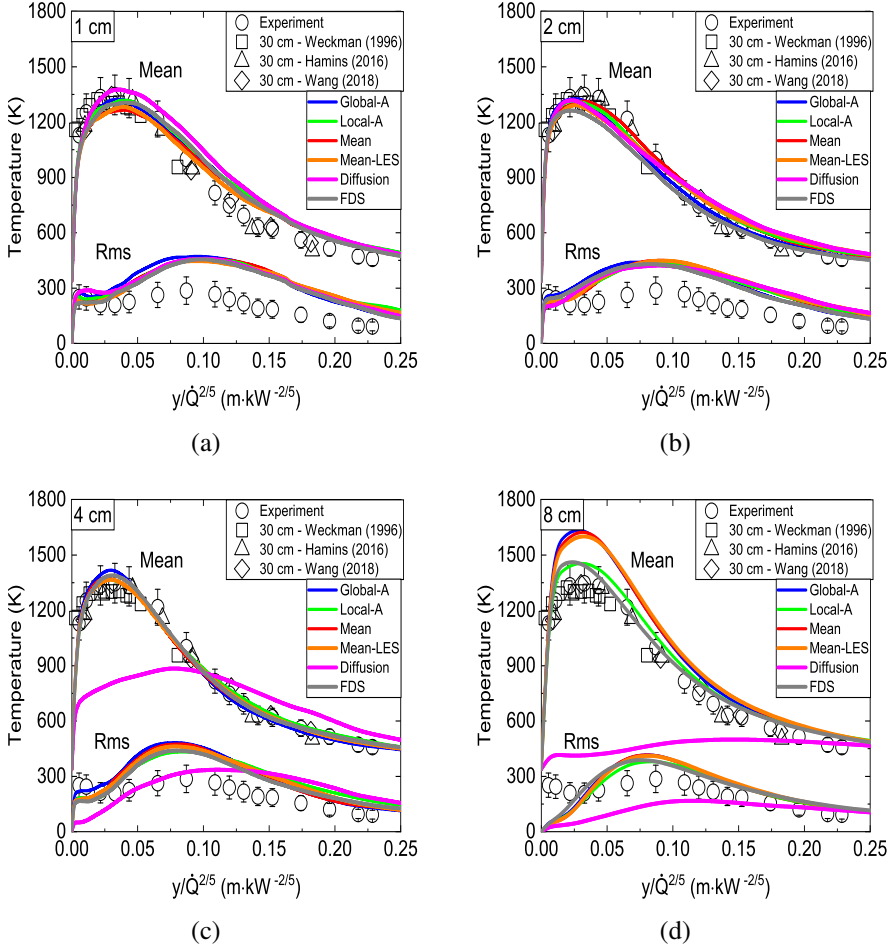


Fig. 7. Centerline mean and rms temperatures using different micro-mixing models with a grid size of (a) 1 cm, (b) 2 cm, (c) 4 cm and (d) 8 cm for the NIST pool fire.

335 can be added as a limit in the calculation of the mixing time scale, τ_{mix} , which will be useful in
 336 scenarios where the sgs quantities approach zero (i.e., DNS limit, laminar flows).

337 6. Conclusions

338 The impact of six sub-grid scale micro-mixing models, used in combination with the Eddy Dissipa-
 339 tion Model (EDM) for combustion, has been considered in the context of buoyancy-driven turbulent
 340 diffusion flames. The models were applied in three different experimental test cases involving
 341 different burner geometries, fire sizes and fuel types.

342 Overall, accurate flame temperature and flow field predictions over a wider range of grid sizes and
 343 test cases were reported which can be attributed to the application of dynamic turbulence models and
 344 the use of a constant radiative fraction which minimized any uncertainties of radiation modelling
 345 on the CFD predictions. In addition, the work illustrated that the micro-mixing model, used in
 346 combination with infinitely fast chemistry in the context of fire simulations, can have a noticeable

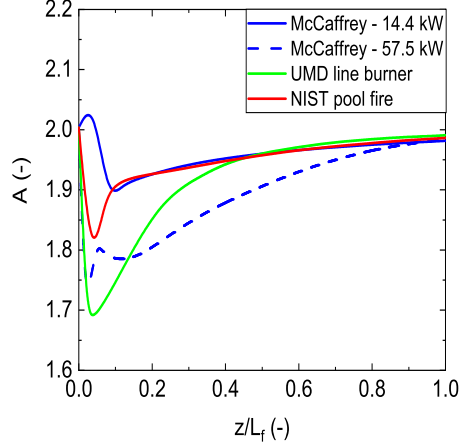


Fig. 8. Average A values using the finest grid sizes in the various test cases.

347 effect on the predicted flame temperatures, particularly when coarser grid sizes are considered. A
 348 key aspect is the dependence of the time scale, used in the micro-mixing model, as a function of the
 349 sgs turbulent Reynolds number. Typical for buoyancy-driven fire flames is that this sgs Re_t number
 350 is low, particularly close to the burner. It was illustrated how the time scales from different micro-
 351 mixing model vary in a significantly different manner in the test cases considered, and how this has
 352 a direct impact on temperature predictions. These differences in the predicted flame temperatures
 353 can potentially lead to discrepancies in the predictions of flame extinction scenarios.

354 Within this context, the best predictions over both coarse and fine grid sizes were obtained by
 355 calculating the mixing time scale as $\tau_{mix} = Ak_{sgs}/\epsilon_{sgs}$ where A varied as a function of the standard
 356 deviation of the mixture fraction (i.e., average value $A \approx 2$), considering a clipped Gaussian shape
 357 for the mixture fraction. Equally accurate were the predictions using the default reaction time
 358 scale model of FDS, which compares the mixing times for diffusion, sub-grid scale advection, and
 359 buoyant acceleration. The other considered time scale models, i.e., based on $\tau_{mix} = Ak_{sgs}/\epsilon_{sgs}$ with
 360 $A = 4$ (i.e., default value of EDM), a time scale model based on the geometric mean of the integral
 361 and the Kolmogorov time scales, a model based on the geometric mean of the sub-grid velocity
 362 stretching time scale and the Kolmogorov time scale, performed satisfactorily on coarse and fine
 363 grid sizes, but tended to significantly over-predict the flame temperatures by up to 300 K on very
 364 coarse grids (in the order of 10 cm). The calculation of the mixing time scale based on the local
 365 variation of the scalar dissipation rate and the mixture fraction variance (i.e., an effective diffusion
 366 time scale) was highly grid-dependent and even though it performed satisfactorily on fine grid sizes,
 367 it strongly under-predicted the flame temperatures on coarser grids. The performance of this model
 368 will also be strongly influenced by the employed turbulence model (i.e., constant or dynamic).

369 7. Acknowledgements

370 This research is funded by The Research Foundation – Flanders (FWO – Vlaanderen) through
 371 project G023221N. We would like to thank Professor Alexander Snegirev for the useful discussions
 372 regarding the EDM combustion model.

373 **References**

- 374 [1] A. Brown, M. Bruns, M. Gollner, J. Hewson, G. Maragkos, A. Marshall, et al., Proceedings of
375 the first workshop organized by the IAFSS Working Group on Measurement and Computation
376 of Fire Phenomena (MaCFP), *Fire Saf. J.* 101 (2018) 1-17.
- 377 [2] G. Maragkos, B. Merci, On the use of dynamic turbulence modelling in fire applications,
378 *Combust. Flame* 216 (2020) 9-23.
- 379 [3] B. Merci, D. Roekaerts, B. Naud, S.B. Pope, Comparative study of micromixing models in
380 transported scalar PDF simulations of turbulent nonpremixed bluff body flames, *Combust. Flame* 146 (2006) 109-130.
- 381 [4] M. Ferrarotti, Z. Li, A. Parente, On the role of mixing models in the simulation of MILD
382 combustion using finite-rate chemistry combustion models, *Proc. Comb. Inst.* 37 (2019) 4531-
383 4538.
- 385 [5] L. Kjäldman, A. Brink, M. Hupa, Micro Mixing Time in the Eddy Dissipation Concept,
386 *Combust. Sci. Technol.* 154 (2000) 207-227.
- 387 [6] P. Moin, K. Squires, W.H. Cabot, S. Lee, A dynamic subgrid-scale model for compressible
388 turbulence and scalar transport, *Phys. Fluids A* 3 (1991) 2746-2757.
- 389 [7] C. Fureby, G. Tabor, Mathematical and Physical Constraints on Large-Eddy Simulations,
390 *Theoret. Comput. Fluid Dyn.* 9 (1997) 85-102.
- 391 [8] B.F. Magnussen, B.H. Hjertager, On Mathematical Modeling of Turbulent Combustion with
392 Special Emphasis on Soot Formation and Combustion, *Proc. Comb. Inst.* 16 (1977) 719-729.
- 393 [9] P. Chatterjee, Y. Wang, K.V. Meredith, S.B. Dorofeev, Application of a subgrid soot-radiation
394 model in the numerical simulation of a heptane pool fire, *Proc. Comb. Inst.* 35 (2015) 2573-
395 2580.
- 396 [10] N. Ren, Y. Wang, S. Vilfayeau, A. Trouvé, Large eddy simulation of turbulent vertical wall
397 fires supplied with gaseous fuel through porous burners, *Combust. Flame* 169 (2016) 194-208.
- 398 [11] G. Maragkos, B. Merci, Large Eddy Simulations of CH₄ Fire Plumes, *Flow Turbul. Combust.*
399 99 (2017) 239-278.
- 400 [12] M.M. Ahmed, A. Trouvé, Large eddy simulation of the unstable flame structure and gas-to-
401 liquid thermal feedback in a medium-scale methanol pool fire, *Combust. Flame* 225 (2021)
402 237-254.
- 403 [13] N. Ren, Y. Wang, A convective heat transfer model for LES fire modeling, *Proc. Comb. Inst.*
404 38 (2021) 4535-4542.
- 405 [14] E.A. Brizuela, R.W. Bilger, On the eddy break-up coefficient, *Combust. Flame* 104 (1996)
406 208-212.
- 407 [15] T. Poinsot, D. Veynante, *Theoretical and Numerical combustion*, Edwards, USA, 2005.

- 408 [16] H. Zhang, E. Mastorakos, LES/CMC Modelling of a Gas Turbine Model Combustor with
409 Quick Fuel Mixing, *Flow Turbul. Combust.* 102 (2019) 909-930.
- 410 [17] R. McDermott, K.B. McGrattan, J. Floyd, A Simple Reaction Time Scale for Under-Resolved
411 Fire Dynamics, *Fire Saf. Sci.* 10 (2011) 809-820.
- 412 [18] K. McGrattan, S. Hostikka, J. Floyd, R. McDermott, M. Vanella, Fire Dynamics Simulator
413 Technical Reference Guide Volume 3: Validation, NIST Special Publication 1018-3, Sixth
414 Edition, 2022.
- 415 [19] J. Chomiak, A. Karlsson, Flame liftoff in diesel sprays, *Proc. Comb. Inst.* 26 (1996) 2557-2564.
- 416 [20] V. Sabelnikov, C. Fureby, LES combustion modeling for high Re flames using a multi-phase
417 analogy, *Combust. Flame* 160 (2013) 83-96.
- 418 [21] C.D. Pierce, P. Moin, Dynamic model for subgrid-scale variance and dissipation rate of a
419 conserved scalar, *Phys. Fluids* 10 (1998) 3041-3044.
- 420 [22] V. Raman, H. Pitsch, A consistent LES/filtered-density function formulation for the simulation
421 of turbulent flames with detailed chemistry, *Proc. Comb. Inst.* 31 (2007) 1711-1719.
- 422 [23] G. Maragkos and B. Merci, A fully dynamic approach for turbulence and combustion mod-
423 ellng: systematic assessment study on fire plumes with variable heat release rate, 12th
424 Mediterranean Combustion Symposium (MCS12), Luxor, Egypt, January 23-26, 2023.
- 425 [24] B.J. McCaffrey, Purely Buoyant Diffusion Flames: Some Experimental Results, National
426 Bureau of Standards, NBSIR 79-1910, 1979.
- 427 [25] J.P. White, E.D. Link, A.C. Trouv , P.B. Sunderland, et al., Radiative emissions measurements
428 from a buoyant, turbulent line flame under oxidizer-dilution quenching conditions, *Fire Saf. J.*
429 76 (2015) 74-84.
- 430 [26] E.J. Weckman, A.B. Strong, Experimental Investigation of the Turbulence Structure of
431 Medium-Scale Methanol Pool Fires, *Combust. Flame* 105 (1996) 245-266.
- 432 [27] K. Sung, J. Chen, M. Bundy, A. Hamins, The characteristics of a 1 m methanol pool fire, *Fire
433 Saf. J.* 120 (2021) 103121.
- 434 [28] G. Maragkos, S. Verma, A. Trouv , B. Merci, Evaluation of OpenFOAM's discretization
435 schemes used for the convective terms in the context of fire simulations, *Comput. Fluids* 232:
436 105208 (2022).
- 437 [29] G. Heskestad, Luminous heights of turbulent diffusion flames, *Fire Saf. J.* 5 (1983) 103-108.
- 438 [30] E.E. Zukoski, B.M. Cetegen, T. Kubota, Visible structure of buoyant diffusion flames, *Proc.
439 Comb. Inst.* 20 (1984) 361-366.

440 **Figure caption list**

- 441 • Fig. 1. Comparison of the different normalised time scales for a grid size of $\Delta = 0.01$ m as a
442 function of the sgs turbulent Reynolds number, Re_t .
- 443 • Fig. 2. Computational domain and local grid refinement used for the (a) McCaffrey's fire
444 plumes, (b) UMD line burner and (c) NIST pool fire.
- 445 • Fig. 3. Centerline excess temperature with (a) 'Global-A', (b) 'Local-A', (c) 'Mean', (d)
446 'Mean-LES', (e) 'Diffusion' and (f) 'FDS' with a 1.5 cm grid size for McCaffrey's plumes.
- 447 • Fig. 4. Centerline excess temperature with (a) 'Global-A', (b) 'Local-A', (c) 'Mean', (d)
448 'Mean-LES', (e) 'Diffusion' and (f) 'FDS' with a 3 cm grid size for McCaffrey's plumes.
- 449 • Fig. 5. Centerline excess temperature with (a) 'Global-A', (b) 'Local-A', (c) 'Mean', (d)
450 'Mean-LES', (e) 'Diffusion' and (f) 'FDS' with a 6 cm grid size for McCaffrey's plumes.
- 451 • Fig. 6. Centerline mean and rms temperatures using different micro-mixing models with a
452 grid size of (a) 0.625 cm, (b) 1.25 cm and (c) 2.5 cm for the UMD line burner.
- 453 • Fig. 7. Centerline mean and rms temperatures using different micro-mixing models with a
454 grid size of (a) 1 cm, (b) 2 cm, (c) 4 cm and (d) 8 cm for the NIST pool fire.